The influence of shallow water on rock armour stability

Scaravaglione, Giulio; Marino, Stefano; Francone, Antonio; Leone, Elisa; Damiani, Leonardo; Tomasicchio, Giuseppe R.; van Gent, Marcel R.A.; Saponieri, Alessandra

DOI
10.1016/j.coastaleng.2024.104657

Publication date
2024

Document Version
Final published version

Published in
Coastal Engineering

Citation (APA)
Scaravaglione, G., Marino, S., Francone, A., Leone, E., Damiani, L., Tomasicchio, G. R., van Gent, M. R. A., & Saponieri, A. (2024). The influence of shallow water on rock armour stability. *Coastal Engineering*, *197*, Article 104657. https://doi.org/10.1016/j.coastaleng.2024.104657

Coastal Engineering 197 (2025) 104657

Contents lists available at ScienceDirect

Coastal Engineering

journal homepage: www.elsevier.com/locate/coastaleng

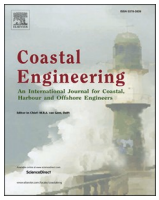

The influence of shallow water on rock armour stability

Giulio Scaravaglione [a], Stefano Marino [b], Antonio Francone [a], Elisa Leone [a], Leonardo Damiani [b], Giuseppe R. Tomasicchio [a], Marcel R.A. van Gent [c], Alessandra Saponieri [a,*]

[a] Department of Engineering for Innovation, University of Salento, Lecce, Italy
[b] Department of Civil, Environmental, Land, Building Engineering and Chemistry (DICATECh), Polytechnic University of Bari, Bari, Italy
[c] Department of Hydraulic Engineering, Delft University of Technology and Deltares, Delft, the Netherlands

ARTICLE INFO

Keywords:
Hydraulic stability
Rubble mound breakwater
Physical model tests
Damage
Shallow water

ABSTRACT

The hydraulic stability of rock armour layers has been extensively discussed in the literature, with numerous formulae proposed for design purposes. However, limited attention has been given to armour stability under shallow water conditions, largely due to the scarcity of experimental data. This research aims to address this gap by providing new insights into the stability of rock armour layers with rubble mound breakwaters in shallow water. Hydraulic stability was determined for four different structure slopes and various hydrodynamic conditions, spanning from deep to extremely shallow water in presence of a 1V:30H foreshore. Newly experimental data were compared with existing stability formulae valid in shallow water, specifically those by van Gent et al. (2003, VG), Eldrup and Andersen (2019, EA), and Etemad-Shahidi et al. (2020, ES). Initially, the data were used to evaluate the accuracy of the original formulae. Following this, the formulae were recalibrated to account for the influence of shallow water, with data grouped according to water levels. Finally, modified versions of VG and ES formulae were developed to fit the experimental data, incorporating the effects of wave steepness to better capture shallow water dynamics.

1. Introduction

Rock-armoured rubble mound breakwaters are the most common coastal structures used to protect harbours and mitigate coastal erosion and flooding. Although the estimation of the hydraulic stability of the armour units is a standard practice for coastal engineers, this calculation may be highly influenced by the stochastic nature of wave loading, movement initiation, and armour damage progression (Campos et al., 2020a, 2020b). The formulae reported in design manuals (e.g., Coastal Engineering Manual (USACE, 2002); Rock Manual (CIRIA/CUR/CETMEF, 2007)) are semi-empirical and primarily based on datasets from 2D physical model tests conducted worldwide.

Rubble mound breakwaters are commonly found along sandy coastlines, especially in shallow water environments. The slopes characteristics of these sandy coasts can vary significantly, ranging from gentle slopes, that allow waves to dissipate energy gradually, to steeper slopes, such as 1V:20H or 1V:30H gradients. These steeper slopes influence wave behaviour and the effectiveness of breakwaters, potentially requiring more robust designs to ensure adequate coastal protection, as they are exposed to depth-limited waves, significantly influenced by seabed. According to the water depth classification of van Gent (1999, 2001), based on the ratio between the spectral wave height in deep water ($H_{m0,o}$) and the water depth at the structure toe (h), namely the relative depth ($h_r = H_{m0,o}/h$), different water depth conditions can be established, ranging from deep (where wave breaking on the foreshore is absent) to extremely shallow foreshores (experiencing a high degree of wave breaking on the foreshore). Specifically, foreshores can be classified as deep ($h_r < 0.40$), intermediate ($0.40 < h_r < 0.75$), shallow ($0.75 < h_r < 1.50$), very shallow ($1.50 < h_r < 3$), and extremely shallow ($h_r > 3$).

Shallow water represents a typical design condition for most coastal structures around the world. They are, for example, prevalent along the U.S. (e.g., the Gulf of Mexico, Melby et al., 2021) and the North Sea (e.g., the sea defence at Scarborough in the U.K., Allsop, 2021) for protecting harbours, navigation waterways, shorelines, and bluffs. Moreover, hard-soft hybrid structures, such as dike-in-dune systems or large beach nourishments in front of sea walls, can be found in the Netherlands and Belgium, where steep foreshores represent a typical average (eroded) profile (Altomare et al., 2020). Such interventions are characterised by large amounts of sand seaward of the hard structure (Altomare et al.,

* Corresponding author.
E-mail address: alessandra.saponieri@unisalento.it (A. Saponieri).

https://doi.org/10.1016/j.coastaleng.2024.104657
Received 29 May 2024; Received in revised form 11 November 2024; Accepted 13 November 2024
Available online 15 November 2024

2016), which can be eroded during extreme storms, potentially altering the water depth conditions at the toe of the structure from intermediate/shallow to very/extremely shallow. In these situations, the impact of wave forces on the structure is strongly influenced by seabed topography and waves are completely different compared to deep water (Allsop et al., 1999; Goda, 2010a,b; Herrera and Medina, 2015). Shallow foreshores are characterised by breaking waves and the release of bound long waves (van Gent, 2001). The energy spectrum tends to flatten and/or become double-peaked, resulting in a prevalence of low frequency components in the surf zone, closely related to the incident wave groups, which increase as waves approach the structure, leading to a reduction in energy at higher frequencies (Kamphuis, 1996; Shah and Kamphuis, 1996).

Shallow water conditions are also expected to become more common with the upgrading of existing breakwaters, driven by changing hydraulic conditions due to sea level rise. In the context of probabilistic design, uncertainties in design conditions under climate change require further research to fully understand wave-structure interaction phenomena and their impact on the functionality of existing rubble mound breakwaters, since these uncertainties could result in the breakwater being unable to meet the design requirements (e.g., Calabrese et al., 2011; Ciardulli et al., 2013; Brancasi et al., 2022; Díaz-Carrasco et al., 2023; Mares-Nasarre et al., 2024). Some possible solutions for upgrading damaged rubble mound breakwaters should be selected based on clear adaptation pathways as highlighted by van Gent and Teng (2023). Despite the practical relevance of upgrading aging structures, limited research has been conducted on the subject (e.g., Burcharth et al., 2014). Currently, no generic method exists to describe the rock armour stability in extremely shallow water conditions, thus requiring a review and update of the current state of knowledge and tools for slope breakwater design, especially in very and extremely shallow water.

To this aim, new 2D experiments have been carried out in the wave flume at the EUropean Maritime and Environmental Research (EUMER) laboratory at the University of Salento (Lecce, Italy) to investigate the effects of shallow water conditions on the hydraulic stability of steep permeable rubble mound breakwaters.

The present paper is organised as follows: **Section 2** presents the literature background, retracing the most relevant findings in rock armour stability over time. **Section 3** describes the physical model setup and performed tests, including the experimental programme and damage measurements. **Section 4** reports the wave analysis of the data collected during the experiments. **Section 5** discusses the results and compares the new experimental data with the available design formulae calibrated for shallow water conditions (van Gent et al., 2003; Eldrup and Andersen, 2019; Etemad-Shahidi et al., 2020). Additionally, modified versions of van Gent et al. (2003) and Etemad-Shahidi et al. (2020) stability formulae for shallow water conditions are proposed to fit the experimental data. Finally, **Section 6** provides a summary of the key findings of the present study and presents perspectives for future research.

2. Background

Early relations describing the incipient motion of seaside armour stones were developed by Iribarren (1938), Hudson (1959) and Losada and Gimenez-Curto (1979), in which the relations differ primarily in the parametric description of the structure slope and friction angle. The widely known Hudson formula has remained the most commonly used method for many decades. At the end of the 1970s and beginning of the 1980s, catastrophic failures were experienced by a series of large rubble mound breakwaters (Scaravaglione et al., 2022), prompting extensive research to improve the design and construction of such structures. Valuable results were achieved by Ahrens (1970), Ahrens and McCartney (1975), and Thompson and Shuttler (1975). The last one recognised the importance of factors as the type of wave breaking, rock placement, and the number of waves, thereby generating a new dataset for flat bottom and impermeable slopes. Results of Thompson and Shuttler (1975) were reanalysed by van der Meer (1988), who performed an extensive laboratory experimental campaign, including both small- and large-scale tests, and quantified the influence of further parameters, i.e., wave period, permeability, storm duration and wave steepness. Based on his extensive dataset, van der Meer (1988) proposed two different formulae for plunging and surging waves, widely employed in the design practice, but mainly limited to deep water. Recently, van der Meer (2021) revisited these equations, as shown in Eqs. (1a,b):

$$N_s = \frac{H_s}{\Delta D_{n50}} = 6.49 c_{pl} P^{0.18} \left(\frac{S}{\sqrt{N_w}}\right)^{0.2} \xi_{s\text{-}1,0}{}^{-0.5} \quad \text{if } \xi_{s\text{-}1,0} < \xi_{s\text{-}1,0,c} \qquad \text{Eq. 1a}$$

$$N_s = \frac{H_s}{\Delta D_{n50}} = 0.97 c_{su} P^{-0.13} \left(\frac{S}{\sqrt{N_w}}\right)^{0.2} \cot\alpha^{0.5} \xi_{s\text{-}1,0}{}^{P} \quad \text{if } \xi_{s\text{-}1,0} \geq \xi_{s\text{-}1,0,c} \qquad \text{Eq. 1b}$$

where:

N_s	stability number
$H_s = H_{1/3}$	significant wave height in the time domain
$\Delta = \rho_r/\rho_w - 1$	relative buoyant density of the rock armour
ρ_r	density of the armour rock
ρ_w	density of the water
$D_{n50} = (M_{50}/\rho_r)^{1/3}$	armour nominal median rock size
M_{50}	median mass of the armour rock grading
α	structure seaward slope angle
$S = A_e/D_{n50}^2$	damage level
A_e	average eroded area (Broderick and Ahrens, 1982)
P	notional permeability factor
g	gravity acceleration
N_w	number of waves in a storm duration
$\xi_{s\text{-}1,0} = \tan\alpha/\sqrt{2\pi H_s/gT_{m\text{-}1,0}^2}$	surf similarity parameter
$T_{m\text{-}1,0}$	negative spectral energy wave period
$\xi_{s\text{-}1,0,c} = \left(\frac{6.49 c_{pl}}{0.97 c_{su}} P^{0.31} \sqrt{\tan\alpha}\right)^{\frac{1}{P+0.5}}$	critical surf similarity parameter
c_{pl}, c_{su}	coefficients that depend on the stone shape (Bradbury et al., 1988; Latham et al., 1988)

These formulae were calibrated using the datasets from Thompson and Shuttler (1975) and van der Meer (1988) and are specifically valid in deep water for a non-sloping seabed. For slopes more gentle than $\cot\alpha = 4$, it is advised to use Eq. (1a), regardless of the value of the surf-similarity parameter. Based on a limited number of tests with breaking waves on the foreshore, van der Meer (1988) suggested replacing H_s with the wave height exceeded by 2 percent of the waves that reach the breakwater ($H_{2\%}$), divided by the ratio $H_{2\%}/H_s = 1.4$ valid for deep water conditions.

Later, Smith et al. (2002) conducted several small-scale laboratory tests to provide more insights into shallow water conditions. This work was extended by van Gent et al. (2003) to recalibrate the formulations proposed by van der Meer (1988), including conditions with shallow foreshores (207 tests). By means of the datasets from van der Meer (1988) and van Gent et al. (2003), modified equations for plunging (Eq. (2a)) and surging (Eq. (2b)) waves were proposed:

$$\frac{H_s}{\Delta D_{n50}} = 8.4 c_{pl} P^{0.18} \left(\frac{S}{\sqrt{N_w}}\right)^{0.2} \xi_{s\text{-}1,0}{}^{-0.5} \left(\frac{H_{2\%}}{H_s}\right)^{-1} \quad \text{if } \xi_{s\text{-}1,0} < \xi_{s\text{-}1,0,c} \qquad \text{Eq. 2a}$$

$$\frac{H_s}{\Delta D_{n50}} = 1.3 c_{su} P^{-0.13} \left(\frac{S}{\sqrt{N_w}}\right)^{0.2} \cot\alpha^{0.5} \xi_{s\text{-}1,0}{}^{P} \left(\frac{H_{2\%}}{H_s}\right)^{-1} \quad \text{if } \xi_{s\text{-}1,0} \geq \xi_{s\text{-}1,0,c} \qquad \text{Eq. 2b}$$

where H_s and $T_{m\text{-}1,0}$ are both computed at the toe of the structure. For slopes more gentle than $\cot\alpha = 4$, it is advised to use Eq. (2a), irrespective

of the value of the surf-similarity parameter.

Using the same database, van Gent et al. (2003) and van Gent (2004) reported an alternative stability formula (Eq. (3)), that does not depend neither on the spectral wave period ($T_{m\text{-}1,0}$) nor the notional permeability factor (P), and includes the nominal rock diameters of both the armour (D_{n50}) and core ($D_{n50,core}$):

$$\frac{H_s}{\Delta D_{n50}} = c_{VG}\sqrt{\cot\alpha}\left(1+\frac{D_{n50,core}}{D_{n50}}\right)\left(\frac{S}{\sqrt{N_w}}\right)^{\frac{1}{5}} \quad \text{Eq. 3}$$

with c_{VG}=1.75.

Physical model tests conducted by Vidal et al. (2006), provided a new formula that depends on the average of the 50 highest waves attacking the structure ($H_{1/50}$). In that study the coefficients proposed by van der Meer (van der Meer, 1988) were recalibrated to design breakwaters in intermediate and shallow water. Lamberti and Tomasicchio (1997) also adopted $H_{1/50}$ to evaluate movement threshold conditions at reshaping berm breakwaters. This approach allows for the consideration of extreme waves that could affect breakwater stability, reducing the risk of damage during extreme storm events and enhancing breakwater safety.

Melby and Hughes (2003) and Melby and Kobayashi (2011) proposed a stability formula based on the maximum wave momentum flux, calibrated with the experimental data of van der Meer (1988). These formulae are based on the physical assumption that wave momentum flux at the toe of the structure is proportional to the maximum wave forces on the armour units, showing that when the water depth is incorporated in the formulation, a better description of stability is obtained.

Herrera et al. (2017) derived a new design formula in presence of breaking waves utilising a combined experimental-numerical approach with the SWAN numerical model (Booij et al., 1999) to compute the incident wave parameters inshore. The authors found that the best fit for their formula is obtained when the spectral wave height (H_{m0}) measured at three times the water depth far from the structure toe ($3h$) is used.

Eldrup and Andersen (2019) investigated the hydraulic stability of a conventional rubble mound breakwater in shallow water, mainly focusing on the effects of nonlinear waves and very low wave steepness. They revisited the original van der Meer stability design formulae (van der Meer, 1988) and developed a new formulation (Eq. (4)), based on the new acquired dataset (68 tests) and the ones provided by van Gent et al. (2003) and Eldrup et al. (2019):

$$\frac{H_{m0}}{\Delta D_{n50}} = c_{EA1}\left(\frac{S}{\sqrt{N_w}}\right)^{0.2} 1.6^{P}\xi_{m\text{-}1,0}{}^{(0.4P-0.67)} \quad \text{plunge if } \xi_{m\text{-}1,0} < \xi_{m\text{-}1,0,c} \quad \text{Eq. 4a}$$

$$\frac{H_{m0}}{\Delta D_{n50}} = c_{EA2}\left(\frac{S}{\sqrt{N_w}}\right)^{0.2} P^{0.17}\min[\cot\alpha, 2]^{0.23} \quad \text{surge if } \xi_{m\text{-}1,0} \geq \xi_{m\text{-}1,0,c} \quad \text{Eq. 4b}$$

where $s_{m\text{-}1,0} = 2\pi H_{m0}/gT^2_{m\text{-}1,0}$ is the wave steepness at the toe of the structure, c_{EA1}=4.5, c_{EA2}=3.1, and the critical surf similarity parameter ($\xi_{m\text{-}1,0,c}$) was redetermined (Eq. (4c)):

$$\xi_{m\text{-}1,0,c} = \left(\frac{c_{EA2}}{c_{EA1}}\frac{P^{0.17}\min[\cot\alpha, 2]^{0.23}}{1.6^{P}}\right)^{\frac{1}{0.4P-0.67}} \quad \text{Eq. 4c}$$

By Eq. (4), a reduction in the uncertainty is achieved, indicating that H_{m0} may be preferable than $H_{1/3}$ or $H_{2\%}$ due to its lower sensitivity to wave nonlinearity.

In Etemad-Shahidi et al. (2020) a multi-variable regression model was used on the experimental database (791 data) available in literature (Thompson and Shuttler, 1975; van der Meer, 1988; van Gent et al., 2003; Vidal et al., 2006), to develop a compact formula applicable across varying water depths for both plunging (Eq. (5a)) and surging (Eq. (5b)) waves:

$$\frac{H_s}{\Delta D_{n50}} = c_{ES1}C_pN_w^{-\frac{1}{10}}S^{\frac{1}{6}}\xi_{s\text{-}1,0}^{-\frac{7}{12}}(1\text{-}3m) \quad \text{if } \xi_{s\text{-}1,0} < 1.8 \quad \text{Eq. 5a}$$

$$\frac{H_s}{\Delta D_{n50}} = c_{ES2}C_pN_w^{-\frac{1}{10}}S^{\frac{1}{6}}\xi_{s\text{-}1,0}^{-\frac{1}{3}}(1\text{-}3m) \quad \text{if } \xi_{s\text{-}1,0} \geq 1.8 \quad \text{Eq. 5b}$$

where $C_p = \left[1+\left(\frac{D_{n50,core}}{D_{n50}}\right)^{3/10}\right]^{3/5}$ represents the permeability coefficient, c_{ES1}=4.5 and c_{ES2}=3.9. These equations incorporate the effect of the foreshore slope (m) and are valid under depth-limited wave breaking conditions.

Losada (2021) questioned the classical methodology used to study the damage evolution of coastal slope structures and proposed a new predictive model, valid also in shallow water conditions, based on a sigmoid function. This approach aims to partially overcome the epistemic uncertainty inherent in the current damage evolution models, by considering the role of the relative depth and, particularly, the interplay between relative depth, wave steepness at the toe of the breakwater, and breakwater slope.

Despite various authors have derived different conclusions regarding the stability of rock armour in shallow water, data for very and extremely shallow water conditions (shallower than those tested or discussed in previous studies such as van Gent et al., 2003, Eldrup and Andersen, 2019, Etemad-Shahidi et al., 2020) remains yet limited and scarce. Therefore, further research and physical model experiments are required to gain a deeper understanding of the effects of shallow water on rock armour stability.

3. New laboratory tests

3.1. Physical model

An experimental investigation was carried out in the wave flume at the EUMER laboratory at the University of Salento (Italy). The wave flume is 45 m long, 2 m high, and 1.4 m wide, equipped with a piston-type wave generator able to generate both regular and second-order irregular waves characterised by target spectra shape (e.g., PM, JONSWAP, TMA, double). The wave generator is equipped with an Active Reflection Compensation system and a mild coarse and rocky spending beach (~1V:10H) is placed at the end of the flume to reduce as much as possible the re-reflection of the flume wall.

A 2D physical model of a rubble mound breakwater (Fig. 1) was built with the toe placed 29.10 m from the wave generator at the end of a 14.30 m long concrete foreshore (m=1V:30H). The foreshore was connected to a flat bottom by means of a short 1.1 m long transitional slope (~1V:5H) ensuring sufficient depth at the wave generator. To ensure proper wave shoaling and breaking along the foreshore and avoid the generation of undesired nonlinear effects due to the presence of the transitional slope, the depth at the end of the transitional slope (h_t in the range 0.59 m–0.94 m) was ensured greater than $0.025L_{p,o}$ (being 3.28 m$\leq L_{p,o} \leq$12.05 m), and the foreshore length greater than 3 local wavelength along the foreshore (Frostick et al., 2011; Eldrup and Andersen, 2024).

During the experimental investigation, wave conditions along the flume were measured through 8 resistive wave gauges (WG_i) with a sampling frequency equal to 40 Hz. Due to the inherent limitations of reflection analysis in depth-limited conditions, all tests were conducted with and without the structure to estimate the incident wave bulk parameters at the toe of the breakwater. Indeed, two different layouts for wave gauges were used: (i) for tests with the breakwater in the flume, and (ii) for wave calibration without the breakwater. The wave gauges

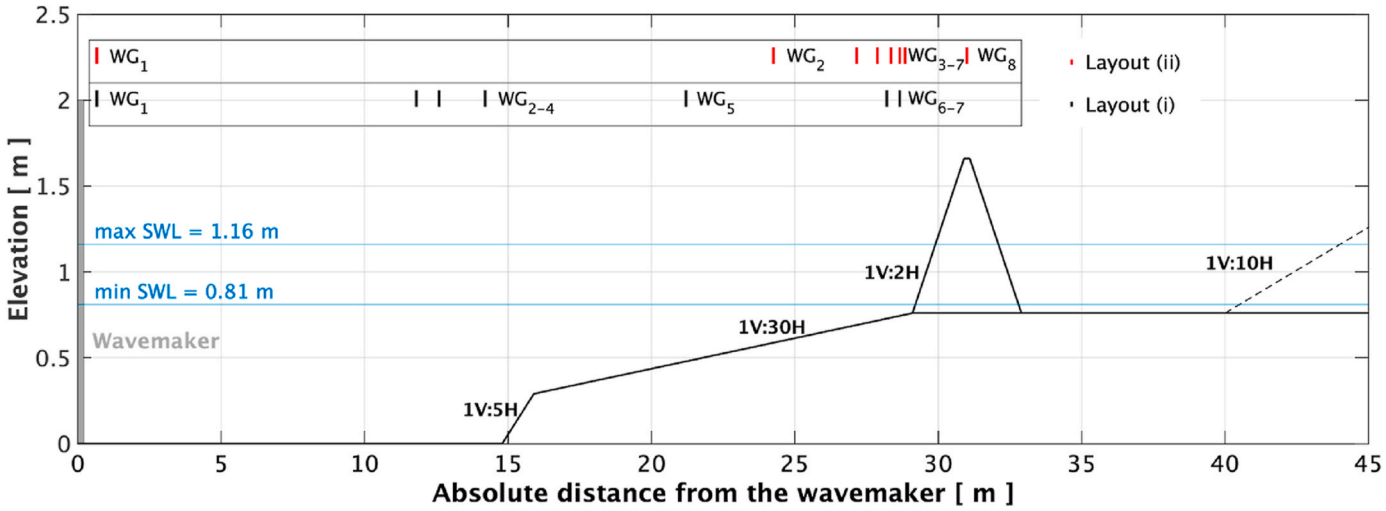

Fig. 1. Cross-section of the physical model and wave gauges (WG_i) locations with (layout (i)) and without (layout (ii)) the breakwater in the flume.

positions for both layouts are detailed in Table 1, providing the absolute distance from the wavemaker.

All the incident variables used in the further analyses refer to the incident wave parameters measured at the WG_6 in layout (ii) (Fig. 1), with no bandpass filter applied to the acquired signals. The incident wave signals were obtained from the calibration tests without the structure in place. This approach was chosen because most methods for separating incident and reflected waves, particularly in the presence of sloping foreshores and nonlinear waves (Lykke Andersen and Eldrup, 2024), fail to capture the true wave behaviour. In fact, uncertainties in determining the incident wave parameters stem from the nonlinear nature of waves, which, in shallow water, transform into breaking rollers. It should be noted that, although the gauge WG_6 is positioned relatively close to the toe, the measured wave height may differ somewhat from the value directly at the toe, which can be approximately 77% of the height recorded at WG_6. These discrepancies arise from the challenges of measuring waves in very shallow water depths, but they fall within the typical uncertainties of physical modelling and are considered acceptable.

The measured free surface elevation from the calibration tests was used to calculate the incident wave parameters, rather than relying on wave separation methods assuming the good performance of the active absorption system. To verify the performance of the absorption system, the measured wave spectra in deep water (WG_1) were compared against the target spectra provided by the wave generation system and with the incident spectra obtained at the $WG_{2\text{-}4}$ array with the model in place (layout (i)), showing reasonable agreement.

The primary drawback of this approach is the introduction of errors caused by wave reflection from the passive absorber during calibration tests. To account for the small but existing reflection induced by the dissipative beach, the inshore bulk reflection coefficient, K_R, was computed for all tests without breakwater in the flume ($0.08 \leq K_R \leq 0.32$), using the method of Mansard and Funke (1980), as modified by Zelt and Skjelbreia (1992), with a four-gauge-array among $WG_{3\text{-}7}$ based on the optimal spacing for the given water and wave conditions.

Since the total waves was measured at a distance of at least one wavelength from the dissipative beach, it was assumed that the incident and reflected waves were uncorrelated, allowing for the calculation of the incident wave height, as suggested by Goda (2010a), using the formula $H_{m0,i}=H_{m0}/(1+K_R)^{1/2}$.

The structure was a conventional non-overtopped rubble mound breakwater without a toe berm. A small wooden slat, approximately 5 mm thick, was fixed seaward on the seabed near the toe, just in front of the bottom row armour rocks. Its purpose was to prevent the stones from sliding over the smooth surface during the tests, ensuring that wave forces acted primarily upslope, roughly 3 to 4 armour units from the toe. Very shallow water are the only scenarios where most of the wave energy is concentrated at the structure toe. In such cases, the presence of the wooden slat may slightly underestimate the observed damage. However, in real-world conditions, stones are likely to encounter resistance from accumulated sand, which is absent in the flume. Thus, these two factors effectively balance each other, aligning the lab results more closely with field conditions.

The breakwater was 0.9 m high with a 0.2 m wide crest. The dimensionless crest freeboard ($R_c/H_{m0,t}$) above the still water level (SWL) was in the range of $1.99 \leq R_c/H_{m0,t} \leq 21.79$, ensuring the avoidance of overtopping conditions. The breakwater was protected by a double armour layer of rocks, randomly placed, with a front/rear slope of α=1V:2H. The armour layers consisted of natural rocks provided by a local quarry. The placement of rocks can be considered bulk-random, and their shape can be assumed as equant and fresh, according to the definition given by Latham et al. (1988). Therefore, in the present work, it can be assumed that no significant differences occurred between expected and predicted results, namely c_{pl}=1.0 and c_{su}=1.0 (van der Meer, 2021). The thickness of the armour and filter layers were determined as $2D_{n50}$ and $0.5D_{n50}$, respectively.

Four breakwater configurations (BW_i) and four water levels (WL_i) were tested across five different test series (Ti), denoted as T1 (BW_1 and WL_1, h=0.40 m), T2 (BW_2 and WL_2, h=0.20 m), T3 (BW_3 and WL_3, h=0.10 m), T4 (BW_4 and WL_3, h=0.10 m), and T5 (BW_4 and WL_4, h=0.05 m) (Fig. 2). Notably, the structure with the highest water depth (T1) was the only configuration with an underlayer composed by stones approximately half the size of those in the armour layer, whereas the other structures consisted of an amour layer atop the core material.

Fig. 3 and Table 2 report, respectively, the sieving curves and the main characteristics of the rocks for each configuration, along with the

Table 1
Wave gauges absolute distance [m] from the wave generator.

Layout	WG_1	WG_2	WG_3	WG_4	WG_5	WG_6	WG_7	WG_8
(i)	0.66	11.8	12.6	13.2	21.2	28.20	28.65	–
(ii)	0.66	24.26	27.16	27.88	28.35	28.65	28.85	31.00

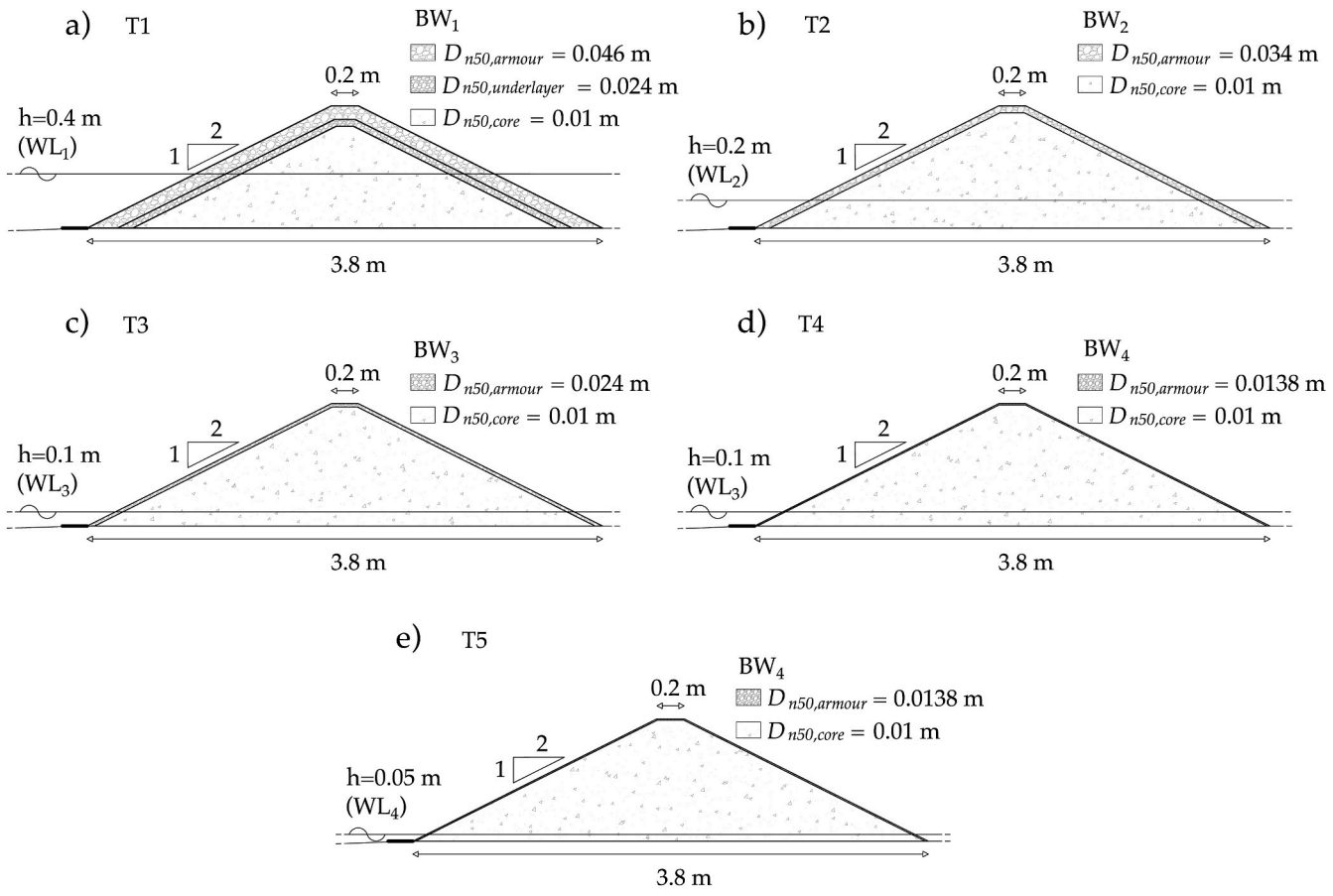

Fig. 2. Layouts of the tested rubble mound breakwaters.

notional permeability factor (P) calculated as proposed by Eldrup et al. (2019). Results show that the structure configuration BW_4 (Figs. 2d,e) closely resembles a homogeneous structure (P=0.55), whereas the cross-sections with the lowest P-values (BW_1 and BW_2 in Figs. 2a,b) are characterised by P-values close to 0.40, in line with the outcomes reported in van der Meer (1988).

Table 2 also reports the $D_{n50,core}/D_{n50}$ ratio, the grading uniformity coefficient (D_{85}/D_{15}), the length-to-thickness ratio (LT), and the blockiness coefficient (BLc) used to assess the grading and the rough angular shape of rock in the armour layers for BW_1, BW_2 and BW_3, following the procedures outlined in the Rock Manual (CIRIA/CUR/CETMEF, 2007). For the BW_4 configuration, the small dimensions of the stones did not permit conducting the same grading and shape characterisation as performed for the other configurations. These parameters were obtained by averaging the values from 20 samples randomly taken from the grain population, as shown in Fig. 4, where the standard deviation (std) for each sample population was also calculated.

The density of the stones was ρ_r=2576 kg/m^3, and the porosity of the core (n) was assumed equal to 0.40 (CIRIA/CUR/CETMEF, 2007). In the present study, the Reynolds number was calculated for both the armour layer (R_{eA}) and inside the porous core (R_{ep}) to assess the flow regime inside the structure and the potential occurrence of scale effects (e.g., Wolters et al., 2009, 2014; Scaravaglione et al., 2024). In intermediate and shallow water R_{eA} exceeds 3x10^4, and, hence, no scale effects are expected. In shallower conditions (i.e., T3, T4 and T5), R_{eA} results 0.75x10^4≤R_{eA}≤2x10^4, indicating that some scale effects could be present. Specifically, for T4 and T5, R_{eA} is slightly lower than 1x10^4, and the test data can be considered slightly conservative, meaning that the corresponding damage to the prototype structure may be slightly less than those observed in the model tests (Hudson, 1975).

3.2. Test programme

A total of 33 tests were conducted to investigate the hydraulic stability of steep rock-armoured rubble mound breakwaters. Experimental tests were grouped for each configuration into two series, each one with increasing wave height and wave period at the generator, while maintaining a constant target offshore spectral wave steepness ($s_{m\text{-}1,0,o}$) equal to 0.024 and 0.048, to simulate a storm with nonstationary conditions. After each test, the structure was always rebuilt before the start of the subsequent test. For each test, a minimum of 1000 waves were generated to examine the initiation and progression of breakwater damage, employing a JONSWAP spectrum with an enhancement factor γ=3.3. For some tests, damage was also measured after 3000 waves, as no significant damage occurred after the initial 1000 waves. Tests were stopped before reaching 1000 waves when the underlayer (for T1) or the core (for T2, T3, T4, T5) became visibly exposed to waves. In such cases, the reduced test duration (t_r) was used to correlate the damage value with the exact number of incident waves, calculated as N_w=t_r/T_m, where T_m is the mean wave period in the time domain. In shallow water, since T_m near the toe of the breakwater may vary and directly impacts the wave count measurement, the N_w in deep water conditions ($T_{m,o}$) was considered. Before each test series, the rubble mound breakwater was exposed to a shake-down test characterised by low energy, to compact the armour rocks and settle the structure (Hughes, 1993).

The data obtained from these experiments encompass tests conducted under intermediate, shallow, very shallow, and extremely shallow water conditions, with and without wave breaking on the foreshore, including also surging and plunging breaking waves. The experimental investigation provided new stability data in very and extremely shallow water (h_r>1.5). Specifically, among the 33 tests, 7 were performed in intermediate (h=0.40 m), 10 in shallow (h=0.20 m),

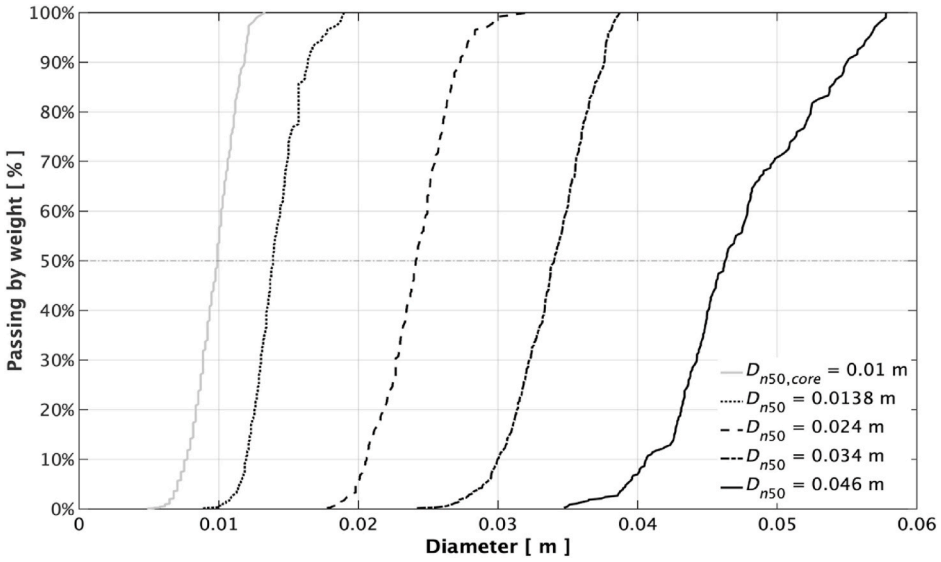

Fig. 3. Rock sieving curves of the rock material used in the experiments.

Table 2
Main characteristics of rocks.

Breakwater configuration	BW_1	BW_2	BW_3	BW_4
D_{n50} [m]	0.046	0.034	0.024	0.0138
$D_{n50,underlayer}$ [m]	0.024	–	–	–
$D_{n50,core}$ [m]	0.01	0.01	0.01	0.01
$D_{n50,core}/D_{n50}$ [-]	0.21	0.29	0.41	0.71
D_{85}/D_{15} – armour [-]	1.26	1.27	1.20	1.28
LT – armour [-]	1.35	1.41	1.46	–
BLc – armour [%]	47.79	36.28	38.18	–
P-values [-]	0.37	0.40	0.47	0.55

10 in very shallow (h=0.10 m), and 6 in extremely shallow water (h=0.05 m).

Table 3 summarises the main characteristics of the experimental programme, including the number of tests for each breakwater configuration (N), the water depth at the breakwater toe (h), the relative depth (h_r), the measured offshore spectral wave steepness ($s_{m-1,0,o}$) and the measured stability number (N_s).

3.3. Damage measurements

Damage measurements were conducted using a high-density laser profiler provided by HR Wallingford. Ten transects were sounded at intervals of 0.10 m across the width of the flume. To avoid boundary-laboratory effects, clearances of 0.20 m and 0.30 m were maintained from the left and right side walls of the wave flume, respectively. In the analysis, the corner of the structure corresponds to the origin of the local reference system (x=0, y=0, z=0), where the x-coordinate represents the longitudinal distance positively towards the external side of the structure, the y-coordinate is the transversal direction positively in the wave propagation direction, and the z-coordinate indicates the vertical direction positively in the upper direction (Fig. 5a). The laser profiler provides a measurement resolution of ±0.5 mm in both the y and z direction, with the same positional accuracy guaranteed by the traverse laser support system (Atkinson and Baldock, 2016; Marino et al., 2022, 2023).

The damage analysis followed similar procedures used by van der Meer (1988) and van Gent et al. (2003), to ensure consistent and reliable comparisons among data derived from different laboratory studies. Profiles were obtained before and after each test, referred to as the mean initial (reference) and final profiles. As explained in **Section 3.2**, the damage was measured after 1000 waves for almost all tests. When failure did not occur after 1000 waves, the test was continued up to 3000 waves (1000+2000), without reconstructing the armour layer.

Fig. 5b illustrates an example of reference and post-1000 wave profiles (test T1), namely the initial and final mean elevation (z) relative to the local reference system (z=0), averaged over the measured transversal transects. The eroded (A_e) and accretion (A_a) areas were calculated as the integral function of the area under the negative and positive

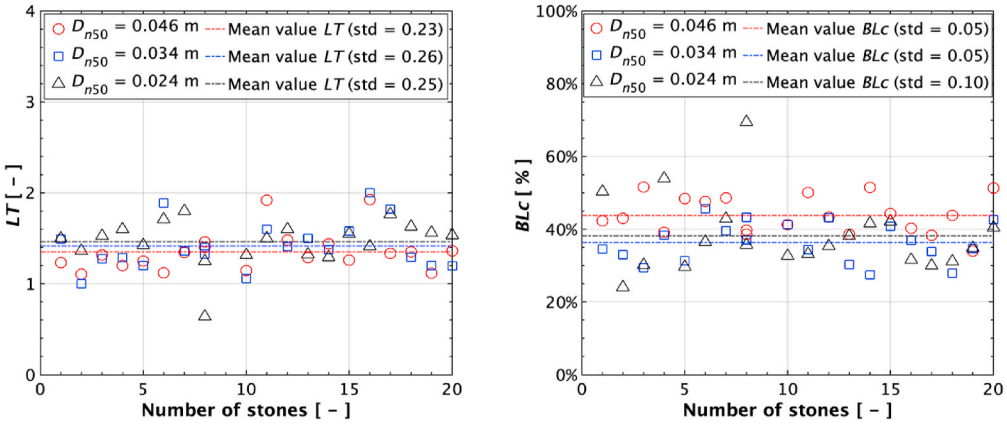

Fig. 4. Shape characterisation of the material used in the experimental campaign: length-to-thickness ratio (on the left) and blockiness coefficient (on the right).

Table 3
Main characteristics of the performed tests.

Test ID	T1	T2	T3	T4	T5
Breakwater configuration	BW_1	BW_2	BW_3	BW_4	BW_4
Water level	WL_1	WL_2	WL_3	WL_3	WL_4
N [-]	7	10	6	4	6
h [m]	0.40	0.20	0.10	0.10	0.05
h_r [-]	0.42–0.75	0.71–1.40	1.49–2.54	1.49–2.03	2.98–4.94
$s_{m\text{-}1,0,o}$ [-]	0.024–0.051	0.025–0.047	0.024–0.046	0.024–0.046	0.024–0.046
$N_s=H_{m0,t}/\Delta D_{n50}$ [-]	2.01–3.44	2.26–2.95	1.47–2.17	2.56–3.39	1.71–2.63

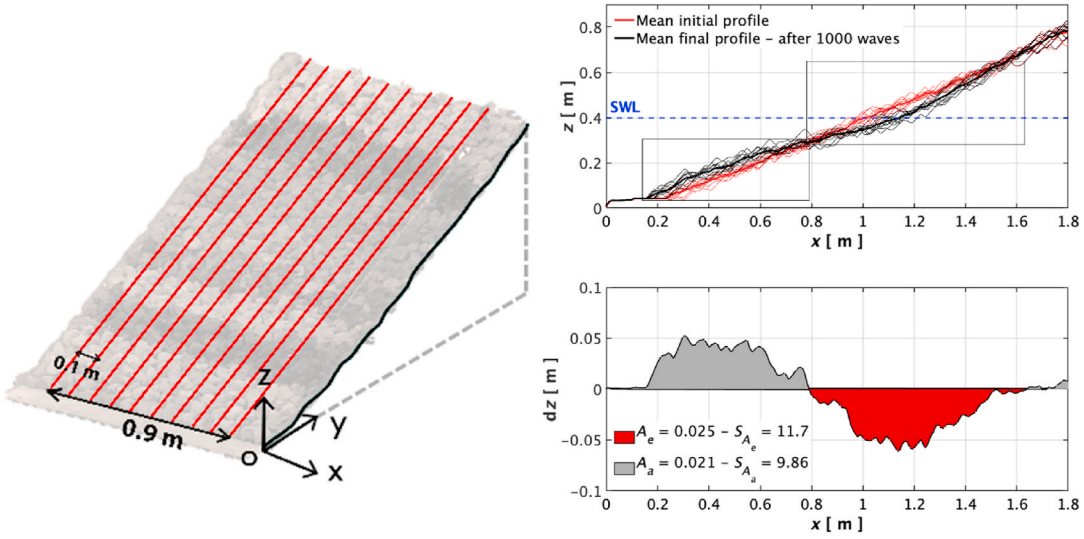

Fig. 5. On the left: Reference coordinate system and 10 transects across the flume width. On the right: Example of reference (red solid lines) and final (black solid lines) averaged profiles measured for the test T1 after 1000 waves (Top right). Spatial evolution of slope elevation changes (dz) with respect to the initial slope (Bottom right): erosion area (red) and accretion area (grey).

values of the average spatial evolution of the slope (dz), also including minor displacements. The damage level S was then estimated as A_e/D_{n50}^2. Table 4 reports the slope damage range measured during the experimental investigation for each test.

Table 4
Measured damage level ranges for each test series.

	T1	T2	T3	T4	T5
Slope damage: S [-]	1.8–20	1.4–11.05	1.3–3	9.6–18.4	1–8.21

4. Wave analysis

The wave analysis was based on the time series of the incident waves recorded in front of the toe of the breakwater without the structure in the flume. Table 5 reports the dimensionless parameters derived from the analyses and the range covered by the entire dataset. In Fig. 6 the measured offshore spectral wave steepness ($s_{m\text{-}1,0,o}=H_{m0,o}/L_{m\text{-}1,0,o}$), the relative wave height ($H_{m0,t}/H_{m0,o}$), the ratio $H_{2\%,t}/H_{s,t}$, and the relative wave period ($T_{m\text{-}1,0,t}/T_{m\text{-}1,0,o}$) are plotted against the relative depth (h_r) computed at the toe of the breakwater.

Previous data from van Gent et al. (2003) covers shallow and very shallow foreshore conditions but does not include low steepness waves, whereas data from Eldrup and Andersen (2019) supplements the van Gent et al. (2003) dataset, also covering smaller wave steepness till to $s_{m\text{-}1,0,o}$=0.01. Fig. 6a shows that new experimental data cover real sea wave conditions (wind waves) in the range $0.02<s_{m\text{-}1,0,o}<0.05$, typically considered in design scenarios. Fig. 6b illustrates that two of the sea states experienced a small amount of shoaling ($H_{m0,t}/H_{m0,o}$ slightly above 1) under relatively intermediate conditions before reaching the structure toe, and hereafter, breaking is observed as the relative depth decreases. In extremely shallow water conditions, the wave height significantly decays up to 20% of the offshore spectral one. Tests involving low steepness waves in shallow foreshore exhibit high nonlinearity and shoaling processes in intermediate water conditions, whereas the others break due to a large wave steepness.

Fig. 6c shows that in deep waters, where wave breaking is absent,

Table 5
Wave characteristics for each test series.

Main parameters	T1 (WL_1)	T2 (WL_2)	T3-T4 (WL_3)	T5 (WL_4)	Total
$H_{m0,o}/h$	0.42–0.75	0.71–1.40	1.49–2.54	2.98–4.94	0.42–4.94
$H_{2\%,t}/H_{s,t}$	1.20–1.37	1.20–1.31	1.29–1.32	1.31–1.43	1.20–1.43
$H_{m0,t}/H_{s,t}$	0.90–0.99	0.89–0.98	0.96–1.04	1.00–1.11	0.89–1.11
$T_{p,o}/T_{m\text{-}1,0,o}$	1.05–1.12	1.02–1.09	1.00–1.09	1.01–1.13	1.00–1.13
$H_{m0,t}/H_{m0,o}$	0.83–1.03	0.57–0.96	0.57–0.96	0.21–0.28	0.21–1.03
$T_{m\text{-}1,0,t}/T_{m\text{-}1,0,o}$	1.00–1.11	1.09–1.36	1.53–2.30	2.42–3.40	1.00–3.40

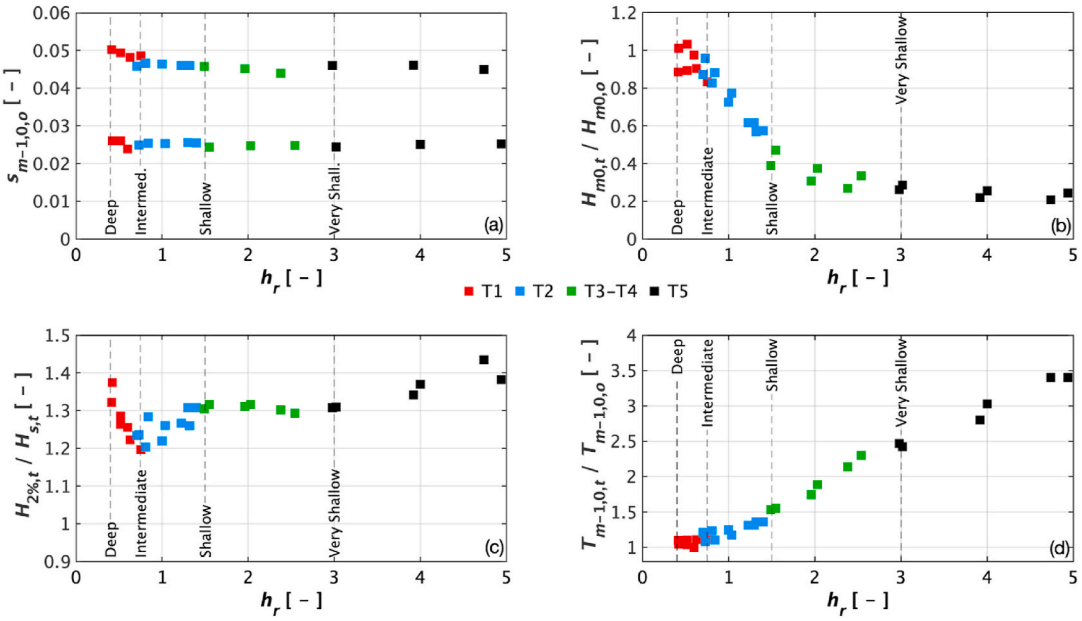

Fig. 6. Wave characteristics as a function of the relative depth.

wave heights can be assumed to be Rayleigh distributed, and the ratio $H_{2\%,t}/H_{s,t}$ tends to 1.40. As waves propagate and shoal towards the shore, nonlinear shoaling process enhances individual wave heights, leading to a deviation in the wave height distribution from the expected Rayleigh distribution. After waves enter the surf zone, the random wave breaking process strongly modifies the wave height distribution. The ratio, indeed, decreases from 1.4 down to 1.2 in shallow water (h_r>0.75), where the ratio begins to increase again and tends to stabilise at very shallow water around 1.3, increasing once more in extremely shallow water (h_r>3) up to 1.40. Consistently with the findings reported by Goda (2010b, 2012), the wave height distribution returns to follow the Rayleigh one as waves approach the shoreline.

The trend of the relative wave period ($T_{m\text{-}1,0,t}/T_{m\text{-}1,0,o}$) against the relative depth is depicted in Fig. 6d. Infragravity (IG) waves in the wave flume are likely to significantly influence wave parameters, especially $T_{m\text{-}1,0,t}$. As waves propagate along the flume, the spectral wave period at the toe increases, reaching nearly four times the deep water period under extremely shallow conditions, due to wave transformation along the foreshore (Hofland et al., 2017). This means that almost all the energy in the proximity of the peak of the spectra is dissipated due to wave breaking at the same time as IG energy is increased and such a behaviour is more pronounced as the relative depth increases, particularly in very and extremely shallow conditions.

Fig. 7 reports the ratio $H_{s,t}/H_{m0,t}$ plotted against the nonlinearity parameter for all tests, corresponding to the two target deep wave steepness values. Goda (2010a,b) described the nonlinearity parameter as $\Pi_0 = \frac{H_{m0,o}}{L_{m,o}} \coth\left(\frac{2\pi h}{L_{m,o}}\right)^3$, where $L_{m,o}$ is the local wavelength calculated with T_m. For $\Pi_0 \leq 0.2$, data show that the ratio $H_{s,t}/H_{m0,t}$ is approximately 1, but a clear difference is observed in the range $0.2 < \Pi_0 < 1$, where $H_{s,t}/H_{m0,t}$ increases, reflecting the expected mean behaviour for low steepness waves according to Goda (2010a,b). For $\Pi_0 \geq 1$, the ratio decreases to around 0.9. In relatively shallow water wave nonlinearity increases with an increase in wave height. As waves approach the shore, they undergo nonlinear shoaling, resulting in wave profiles with high and sharp crests and low and flat troughs. This nonlinearity effect becomes most pronounced around the outer edge of the surf zone. Within the surf zone, waves begin to break, and nonlinearities are gradually lessened, in accordance with wave steepness. Specifically, low steepness waves experience significant nonlinear shoaling before breaking, whereas high steepness waves break earlier.

Fig. 8 provides further insights into the energy spectral spreading during wave propagation in shallow water by showing the ratio $m_{0,t}^{IG}/m_{0,t}^{TOT}$ at varying relative depth, where $m_{0,t}^{IG}$ represents the infragravity (IG) wave energy component, and $m_{0,t}^{TOT}$ represents the total wave energy, both evaluated at the structure toe. The inset plot shows an example of the density spectrum for a test in very shallow water (T4),

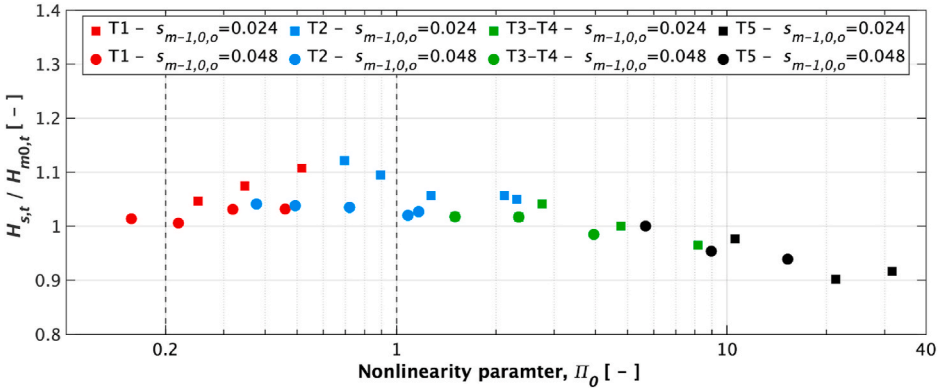

Fig. 7. Wave height ratio as a function of the nonlinearity parameter.

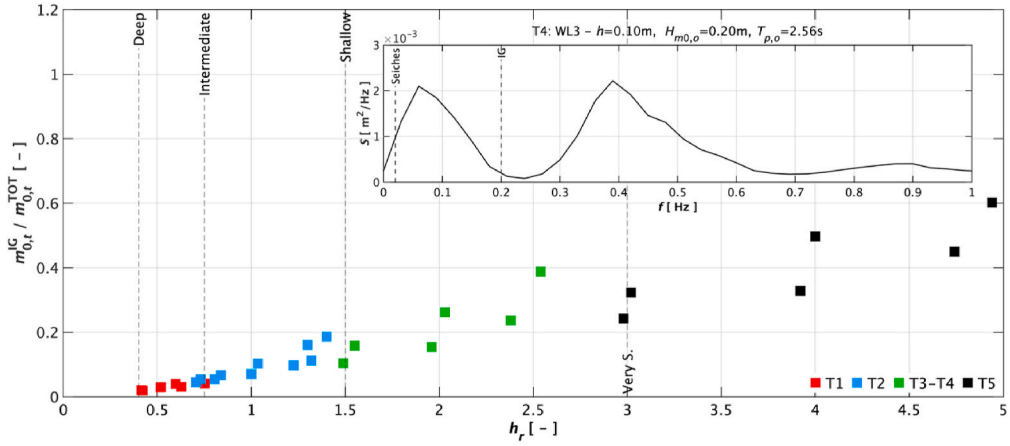

Fig. 8. Ratio $m^{IG}_{0,t}/m^{TOT}_{0,t}$ as a function of the relative depth. The inset plot reports an example of the energy density spectrum for T4, at the wave gauge WG_6.

evaluated at the toe, highlighting the dominant peak frequencies. As water depth decreases, wave breaking begins, causing dissipation of energy at the peak and higher harmonic frequencies, while energy at lower frequencies continues to increase. Due to the very long wavelengths of these low-frequency waves, they do not break, and the substantial energy present at these lower frequencies explains the observation of large wave periods in shallow water. The spectrum clearly indicates significant energy in the infragravity frequency band in very shallow water. Results, indeed, demonstrate that, in the deep water, the infragravity waves minimally contribute to the total wave energy, but this contribution becomes progressively more significant as the water depth decreases. The most noticeable increase in the ratio occurs in extremely shallow water, where $m^{IG}_{0,t}/m^{TOT}_{0,t}$ values are the highest and the energy of IG components reach also the 60% of the total wave energy.

In Fig. 9 the spectral wave steepness computed at the toe of the structure is reported as a function of the relative depth (h_r). It was computed using $H_{m0,t}$ and $L_{m\text{-}1,0,t}$, where $L_{m\text{-}1,0,t}$ was calculated using the deep water wavelength formula, with the spectral wave period at the toe ($T_{m\text{-}1,0,t}$). Since the spectral shape changes significantly in extremely shallow water the wave steepness becomes very low. The increased energy at lower frequencies results in an exceptionally large spectral wave period. However, it is important to emphasise that the total wave steepness is dominated by the energy at the lower frequencies making it less representative of the wave field and the steepness of the short waves. As expected, the wave steepness ratio ($s_{m\text{-}1,0,o}/s_{m\text{-}1,0,t}$) increases from intermediate to extremely shallow water conditions. However, it should be noted that in such conditions, waves break over a wide surf zone on the foreshore and not directly on the structure slope.

In Table 6, the datasets utilised for the calibration of the stability formulae compared with the new experimental data (van Gent et al., 2003; Eldrup and Andersen, 2019; Etemad-Shahidi et al., 2020), are reported together with the range of the main parameters explored in this experimental investigation. Specifically, the new dataset covers ranges of the relative water depth at the structure toe (h_r) from 0.42 to approximately 5, extending the previous range of investigation.

5. Results

5.1. Damage analysis

The relationship between damage values (S) and stability numbers

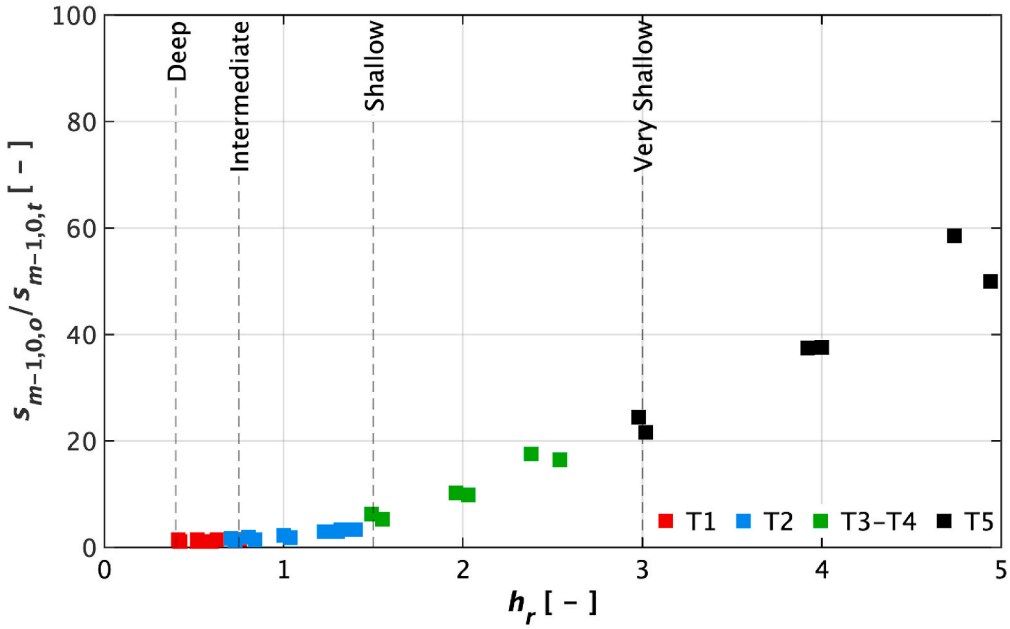

Fig. 9. Influence of the relative depth on $s_{m\text{-}1,0,o}/s_{m\text{-}1,0,t}$ for different shallowness conditions.

Table 6
Range of parameters used for calibrating design formulae.

	Rock stability formulae valid in shallow water conditions			
	Van Gent et al. (2003)	Eldrup and Andersen (2019)	Etemad Shahidi et al. (2020)	Present study
Datasets used for stability formulae calibration	Van der Meer (1988) Van Gent et al. (2003)	Van Gent et al. (2003) Eldrup et al. (2019) Eldrup and Andersen (2019)	Van der Meer (1988) Thompson and Shuttler (1975) Van Gent et al. (2003) Vidal et al. (2006)	EUMER
Parameters				
Structure slope angle: cotα	1.5–6	1.5–4	1.5–6	2
Foreshore slope angle: cot$m$	Flat, 30, 100	30, 100	Flat, 30, 100	30
D_{n50} [m]	0.022–0.21	0.022–0.044	0.0164–0.21	0.0138–0.046
$D_{n50,core}/D_{n50}$	0.0–1.0	0.0–0.45	0.0–1.0	0.21–0.71
Relative mass density: Δ	0.90–2.05	1.62–1.75	0.92–2.05	1.576
Notional permeability: P	0.10–0.60	0.10–0.50	0.1–0.6	0.37–0.55
Offshore wave steepness: $s_{m,o}$	0.004–0.064	0.009–0.063	0.004–0.081	0.020–0.049
Offshore surf similarity parameter: $\xi_{m,o}$	0.67–7.58	1–6.77	0.67–7.58	2.26–3.54
Relative depth at the structure toe: h_r	0.058–1.5	0.18–1.5	0.038–1.5	0.42–4.94
Stability number: N_s	0.7–4.38	0.7–4.27	0.7–4.38	1.47–3.44
Slope damage: S	<62	<62	<62	1.01–20.03
Number of waves: N_w	<3 000	492–5 172	492–5 172	652–4 064
Number of data: N	579 + 207	207 + 68	791	55

(N_s) computed at the toe of the breakwater is typically represented by a power relationship (Eq. (6)):

$$S = a(N_s)^b \quad \text{Eq. 6}$$

where a and b are regression coefficients calibrated using measured values through the nonlinear least squares method. Specifically, the coefficient b defines the shape of the damage curve and has been recognised as the reference coefficient for comparing damage curves from different datasets. Van der Meer (2021) has underlined that a proper comparison among damage results from different experimental investigations is possible if the exponents of the damage curves are comparable. Hence, in the present work, the same methodology described by van der Meer (1988) was replicated to derive the coefficient of the damage fitting curve from the new experimental data. Overall, the exponent b was found to fall within the range $4.09 \leq b \leq 5.07$, yielding shape factors for the damage curve ranging from $S=f(Ns^4)$ to $S=f(Ns^5)$ similar to previous studies, where $b=5$ was found. In the analyses, S-values in the range $1 \leq S \leq 15$ were considered, as larger values fall outside the range of practical relevance. Accordingly, in Fig. 10 the experimental damage curves are plotted against the stability number for both deep target steepness along with the 5-power regression line (dotted curve) for each breakwater configuration (BW_i). Results show that, as expected, in all tests the damage increases as the stability number increases and no evident differences can be observed between the two wave steepness values. For the BW_4 configuration tested at two different water levels (WL_3 and WL_4), it was observed that, despite the same structure configuration, the stability behaviour varied under different water level conditions likely because different wave steepness do not follow the same stability curve in deep water, and therefore it is not expected they would in shallow water either.

The following subsections present the analyses on the influence of shallow water conditions on the stability of a rock-armoured steep breakwater. This is achieved by evaluating the accuracy of the formulae developed by van Gent et al. (2003) (VG, Eq. (3)), Eldrup and Andersen (2019) (EA, Eqs. (4a,b)), and Etemad-Shahidi et al. (2020) (ES, Eqs. (5a, b)) against newly acquired experimental data. First, the accuracy of the original formulae is assessed relative to this new data. Then, the formulae are recalibrated to account for shallow water conditions, with

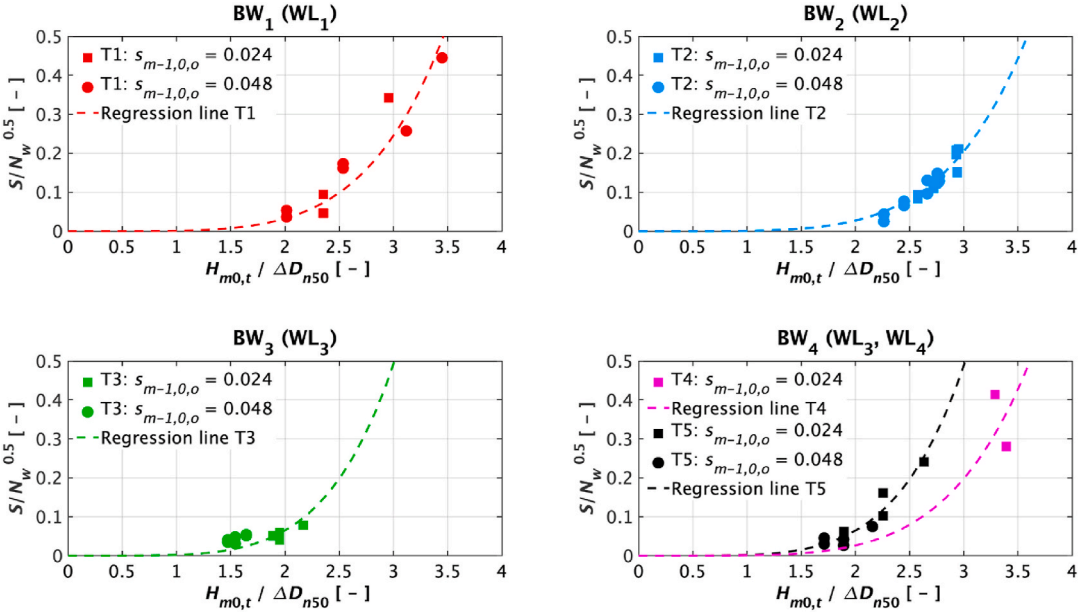

Fig. 10. Slope armour damage S against the stability number $N_s=H_{m0,t}/\Delta D_{n50}$.

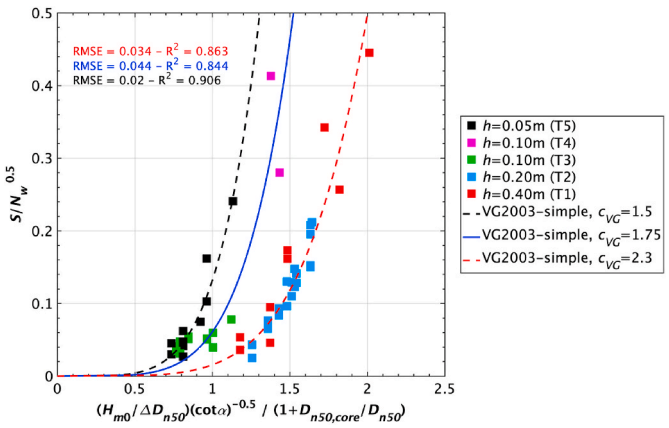

Fig. 11. Refitting of the van Gent et al. (2003) formula with the new data.

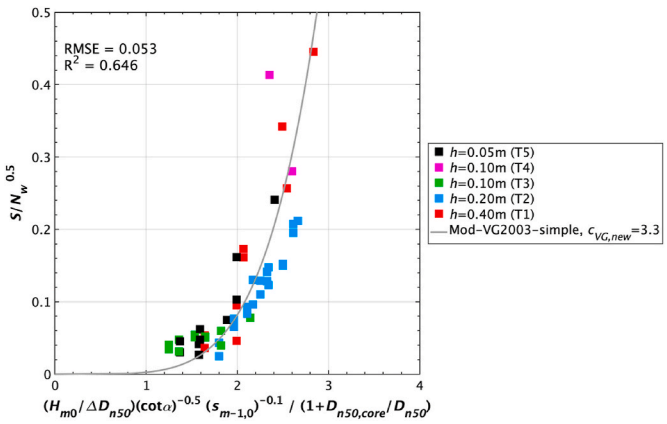

Fig. 12. Refitting of the simple formula of van Gent et al. (2003) according to Eq. (7).

the data categorised by water levels and new regression coefficients calculated. Modified versions of the VG and ES formulas are also explored to fit the new experimental data and are specifically valid for the range of application investigated here, incorporating the incident wave steepness to better capture the effects of shallow water.

5.2. Comparison with existing formulae valid in shallow water

5.2.1. Van Gent et al. (2003)

Fig. 11 reports the observed dimensionless damage according to the VG expression (Eq. (3)), with the experimental data aggregated into 4 groups based on the investigated water levels: intermediate (red squares, h=0.40 m), shallow (blue squares, h=0.20 m), very shallow (green and magenta squares, h=0.10 m), and extremely shallow (black squares, h=0.05 m) water. The theoretical curve (blue line, with c_{VG}=1.75) derived from Eq. (3) is also plotted. With respect to the theoretical regression line, a good prediction of damage is observed for very shallow water (tests T3 and T4) in both breakwater configurations (BW_3 and BW_4) at the same water level, regardless of the permeability. However, an overestimation of the predicted damage for intermediate/shallow water (tests T1 and T2), and an underestimation of damage for extremely shallow water (test T5) are observed. Therefore, for each water level, the formula was refitted to derive a new regression coefficient c_{VG}, to better fit the experimental data. In these analyses, the time-domain significant wave height (H_s) is replaced with the significant spectral one (H_{m0}) to minimise the influence of spectral shape and wave nonlinearity effects compared to low exceedance time domain wave heights (e.g., H_s or $H_{2\%}$). Moreover, frequency-based parameters (H_{m0} and $T_{m-1,0}$) are commonly used in practical design and typically derived from numerical wave models, making them readily available without relying on empirical relations, unlike time domain parameters that necessitate detailed knowledge of the wave height distribution.

Results show that data in intermediate (h=0.40 m) and shallow (h=0.20 m) water exhibit similar behaviour (red dotted line, c_{VG}=2.3) and can be clustered, whereas data in extremely shallow water (h=0.05 m) are well represented by Eq. (3) if a regression coefficient c_{VG} equal to 1.5 is used (black dotted line).

From these results, the primary conclusion is that data corresponding to different water levels at the toe of the structure do not converge into a single formula and exhibit high uncertainty when c_{VG}=1.75 is applied uniformly for all data. Therefore, Eq. (3) can be adjusted to account for the effects of shallow water conditions. Fig. 11 shows that the recalibrated van Gent formula exhibits a better agreement with the experimental data if different water levels are considered separately. In this context, the influence of the spectral wave period becomes evident.

Based on these findings, a new formula is developed to fit the new experimental dataset and provide better insights into the effects of shallow water. Eq. (3) was modified by adding the influence of the spectral wave steepness (wave period) as a function of H_{m0}. All incident wave parameters were computed at the toe of the structure and $s_{m\text{-}1,0}$ was calculated using the deep water wavelength formula, considering the incident wave parameters. Results are reported in Fig. 12 and demonstrate that the modified formula (Eq. (7)), provides a better prediction of the observed damage for the new dataset if a regression coefficient $c_{VG,new}$ equal to 3.3 is used, across the different shallowness conditions investigated in the present study.

$$\frac{H_{m0}}{\Delta D_{n50}} = c_{VG,new}\sqrt{\cot\alpha}\left(1+\frac{D_{n50,core}}{D_{n50}}\right)s_{m\text{-}1,0}^{0.1}\left(\frac{S}{\sqrt{N_w}}\right)^{\frac{1}{5}} \qquad \text{Eq. 7}$$

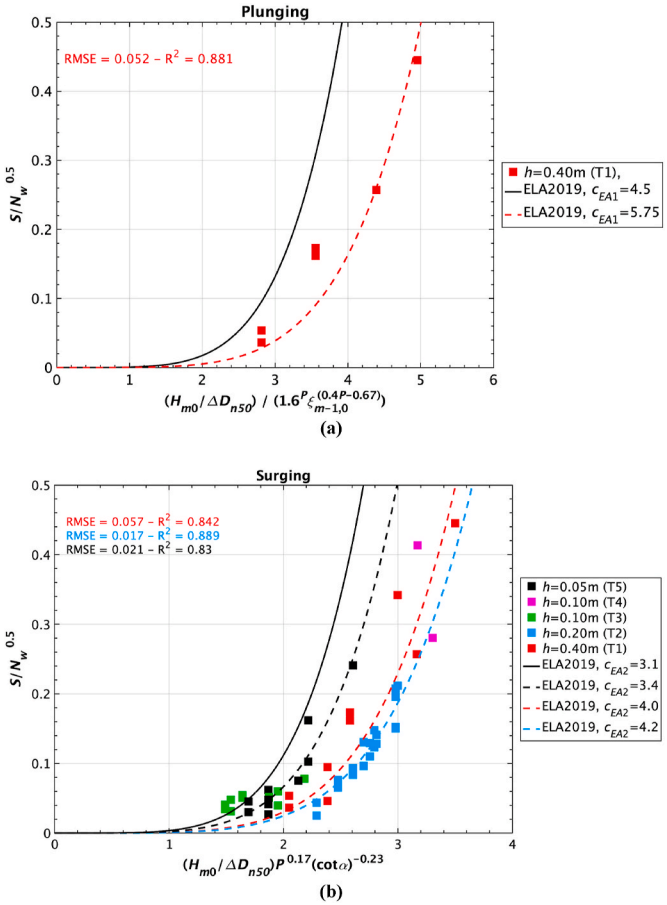

Fig. 13. Refitting of the Eldrup and Andersen (2019) stability formula for different shallowness conditions: a) plunging waves; b) surging waves.

5.2.2. Eldrup and Andersen (2019)

Fig. 13 presents the new data plotted alongside the stability formulae proposed by Eldrup and Andersen (2019) (EA, Eq. (4)). For each breakwater configuration, the permeability factor P, reported in Table 3, was estimated based on the method proposed by Eldrup et al. (2019).

Results show that only a few tests in intermediate waters experience plunging breaking waves on the structure (Fig. 13a), whereas all the other data experienced surging breaking conditions (Fig. 13b). The observed dimensionless damages are calculated using Eqs. (4a,b), shown in Fig. 13a,b, respectively, where the black solid curves represent the theoretical predicted damage, with a regression coefficient c_{EA1} equal to 4.5 in plunging breaking conditions and c_{EA2} equal to 3.1 in surging ones. Results reveal that, in both breaking conditions, the predictions generally overestimate the observed damage, and such a difference increases as the damage level increases. In surging conditions, the empirical equation aligns better with the observed low damage values in very and extremely shallow water conditions (black and green squares), even if the bias increases in extremely shallow water when the structure is subjected to higher damage levels. In all other conditions, the predicted damage is overestimated. In both graphs, the recalibrated regression lines based on the newly acquired data are shown, showing a better fit with a regression coefficient c_{EA1} equal to 5.75 for plunging conditions in intermediate waters, and c_{EA2} equal to 3.4, 4.0 and 4.2 for very shallow, intermediate and shallow conditions, respectively.

5.2.3. Etemad-Shahidi et al. (2020)

A similar comparison was also conducted using the stability formula proposed by Etemad-Shahidi et al. (2020) (ES, Eq. (5)). Fig. 14 reports the new data plotted according to Eq. (5b), namely for surging conditions, since $\xi_{m\text{-}1,0,t} \geq 1.8$ is observed for the entire dataset. Also in this case, the primary conclusion remains that new data, referring to different water levels, do not tend to collapse into a single cluster and are overestimated by the original formula with a regression coefficient c_{ES2} equal to 3.9. Experimental data under intermediate conditions show less deviation from predictions compared to other shallowness conditions. Thus, data were grouped by water levels, and the new regression coefficients were determined for the original equation. Specifically, results demonstrate a good estimation of damage for deep, shallow, and very and extremely shallow water conditions with c_{ES2}=4.56 (dotted red line), c_{ES2}=5.45 (dotted blue line), and c_{ES2}=6.98 (dotted black line), respectively. In this last case, very shallow (h=0.10 m) and extremely shallow (h=0.05 m) conditions exhibit the same behaviour and were aggregated. As with the VG equation, the effect of the spectral wave steepness was incorporated into the formulation, specifically aimed to fit the new experimental dataset, as reported in Eq. (8):

$$\frac{H_{m0}}{\Delta D_{n50}} = c_{ES,new} C_p N_w^{-\frac{1}{10}} \cot\alpha^{\frac{1}{3}} S^{\frac{1}{6}} s_{m\text{-}1,0}^{\frac{1}{20}} \quad \text{surge if } \xi_{m\text{-}1,0} \geq 1.8 \qquad \text{Eq. 8}$$

Results shown in Fig. 15 demonstrate that incorporating the spectral wave steepness into the model leads to a good correlation between the data and the expression for all conditions with $c_{ES,new}$=3.55 (Eq. (8)). In the original formulation, the spectral wave steepness is explicitly incorporated within the surf similarity parameter. In this approach, the structure slope and wave steepness are treated as separate variables, as the surf similarity parameter may not be the most effective parameter for characterising both influences simultaneously. This new formulation was necessary, particularly under shallow water conditions, to recalculate both the regression coefficient $c_{ES,new}$ and the power exponent of the wave steepness, which was observed to differ from the exponent of the surf similarity parameter. As for the VG formulation, the wave steepness power was incorporated into the ES equations by first establishing its physical influence, given the direct proportionality of the stability number (N_s) to wave steepness ($s_{m\text{-}1,0}$), and then calibrating the optimal exponent to fit the new experimental data.

6. Conclusions and future perspectives

Rock armour stability has been studied using physical model experiments with rubble mound breakwaters in shallow water with various hydrodynamic conditions with severe wave breaking along a 1V:30H foreshore. Four distinct breakwater configurations and water levels were tested, ranging from deep to extremely shallow foreshores, for a total of 33 tests. The aim was to investigate the influence of very and extremely shallow water conditions (h_r up to 5), which have hardly been tested systematically before. The experimental results were utilised to assess the performance of existing stability formulae specifically designed for such conditions, namely those proposed by van Gent et al. (2003) (VG), Eldrup and Andersen (2019) (EA), and Etemad-Shahidi et al. (2020) (ES) using the newly obtained data. Initially, the accuracy of the original formulae was tested against the experimental findings, highlighting discrepancies in their performance. To address these issues, the formulae were recalibrated grouping the data based on water levels,

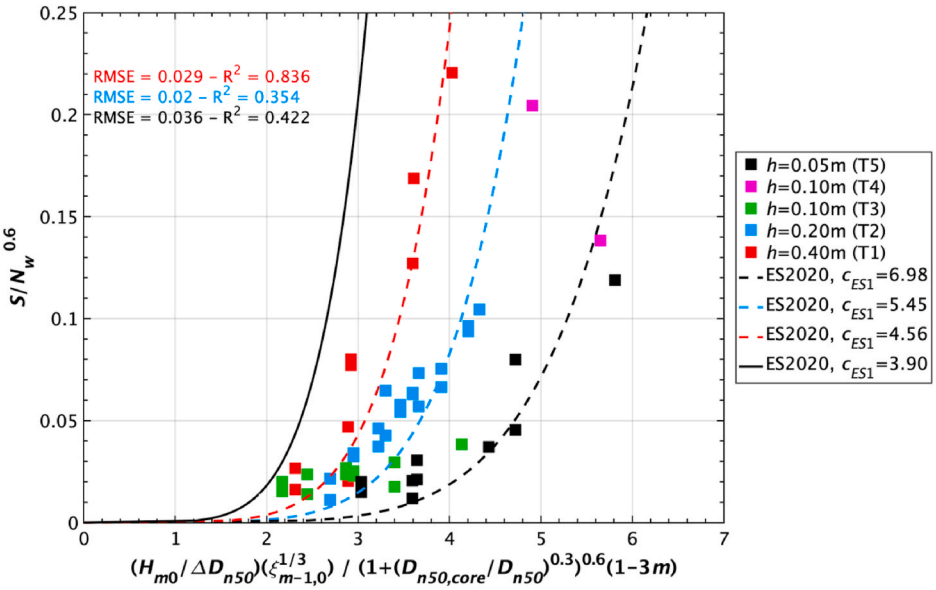

Fig. 14. Refitting of the Etemad-Shahidi et al. (2020) stability formula with the new data.

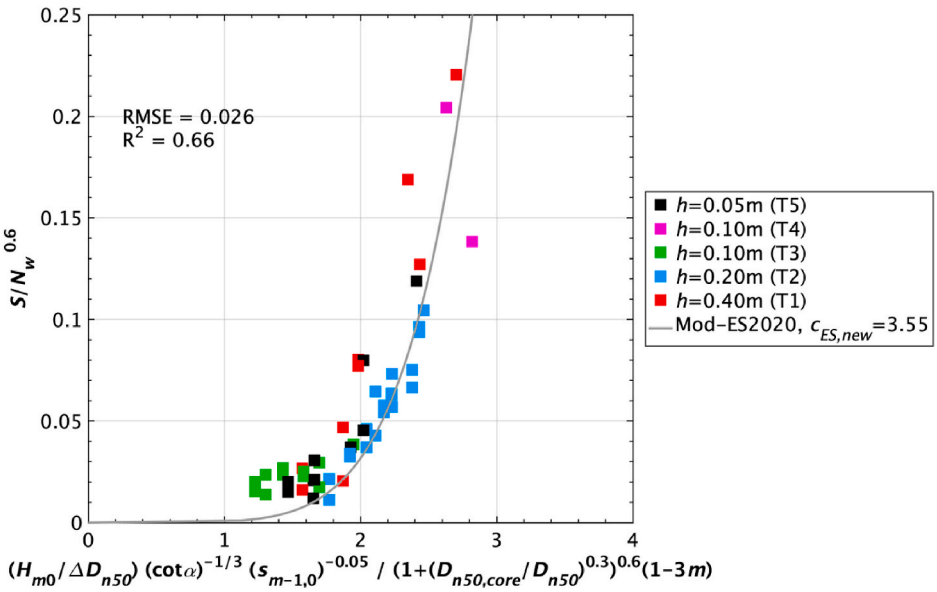

Fig. 15. Refitting of the Etemad-Shahidi et al. (2020) stability formula according to Eq. (8).

and new regression coefficients were derived to better fit the new experimental data. Additionally, modified versions of the VG and ES formulae were developed to account for the effects of incident wave steepness, improving their ability to reflect shallow water dynamics.

The application of the original formulation by VG to the new data reveals that data pertaining to different water levels at the toe of the structure do not converge into a single formula and exhibit significant uncertainty when a unique coefficient (c_{VG}=1.75) is applied. While a reliable estimation of damage for very shallow water was noted, there was an overestimation of the predicted damage for intermediate and shallow water, and an underestimation in extremely shallow water. This means that the influence of shallow water is not properly incorporated in the stability equation. Therefore, for each water level, the formula was recalibrated to derive new regression coefficients c_{VG}, depending on water levels, showing that data in intermediate and shallow water exhibited similar behaviour (c_{VG}=2.3), whereas data in extremely shallow water were well predicted if a regression coefficient c_{VG}=1.5 was used. For our dataset, a more accurate prediction of the observed damage was achieved if the influence of the incident wave steepness was considered. Indeed, a new equation (Eq. (7)) was derived specifically valid in shallow water with $c_{VG,new}$=3.3.

Discrepancies between observed and predicted damage were noted also for the formulae proposed by Eldrup and Andersen (2019) and Etemad-Shahidi et al. (2020). For EA formulation, the comparison among predicted and observed damage measurements showed that, in both surging and plunging breaking conditions, the predictions generally tended to overestimate the observed damage as the damage level increases. Under surging conditions, the observed damage was more accurately predicted especially for low S-values in very and extremely shallow water. The bias grew in extremely shallow water when the structure experienced higher damage levels. The recalibration of the formula, based on the new acquired data, showed a better fit with a regression coefficient c_{EA1}=5.75 for plunging conditions in intermediate waters, and c_{EA2} equal to 3.4, 4.0 and 4.2 for very shallow, intermediate and shallow conditions, respectively.

The stability formula proposed by Etemad-Shahidi et al. (2020) (Eq. (5)), applied to surging conditions for the entire dataset, showed that the main finding remained consistent. The new data, corresponding to different water levels, did not converge into a single cluster and were generally overestimated. In intermediate conditions, a lower bias was observed compared to the other water levels. Consequently, new regression coefficients were calculated, providing accurate damage estimates for deep, shallow, very/extremely shallow conditions with coefficients c_{ES2} equal to 4.56, 5.45, and 6.98, respectively. As with VG equation, the impact of wave steepness was integrated into the formula (Eq. (8)), resulting in a good prediction of the new data with $c_{ES,new}$=3.55. In this context, the structure slope and wave steepness were treated as separate variables, as the surf similarity parameter may not be the most effective parameter for characterising both influences simultaneously.

It is important to emphasise that the dataset used in this study is relatively small and is closely tied to particular wave conditions and structural layouts. This limitation poses challenges when attempting to generalise the derived equations to broader contexts. Consequently, further experiments are necessary, particularly under very shallow and extremely shallow water conditions, while also accounting for varying foreshore and structure slopes. This will allow for a more comprehensive evaluation of the proposed formulae, ultimately enhancing their utility and reinforcing their applicability in real-world engineering applications.

CRediT authorship contribution statement

All the authors contributed in equal measure to all states of the development and production of this paper.

Declaration of competing interest

The authors declare that they have no known competing financial interests or personal relationships that could have appeared to influence the work reported in this paper.

Acknowledgments

This work was funded by *Piano Nazionale di Ripresa e Resilienza (PNRR), Missione 4 Istruzione e Ricerca, Componente C2, Investimento 1.1 Fondo per il Programma Nazionale di Ricerca e Progetti di Rilevante Interesse Nazionale (PRIN), Research project A PRObabilistic fraMEwork for coasTal and harbor dEfense in the cOntext of climate change, PROMETEO (P20224T9SK)*.

Data availability

Data will be made available on request.

References

Ahrens, J.P., 1970. The influence of breaker type on riprap stability. Coast. Eng. Proceed. 1970.

Ahrens, J.P., McCartney, B.L., 1975. Wave Period Effect on the Stability of Riprap.

Allsop, N.W.H., Durand, N., Hurdle, D.P., 1999. Influence of steep seabed slopes on breaking waves for structure design. Coast. Eng. Proceed. 1998, 906–919. https://doi.org/10.1061/9780784404119.067.

Allsop, N.W.H., 2021. Old British Breakwaters: How Have Engineering Developments Influenced Their Survival? *Doctoral Dissertation*. University of Edinburgh.

Altomare, C., Suzuki, T., Chen, X., Verwaest, T., Kortenhaus, A., 2016. Wave overtopping of sea dikes with very shallow foreshores. Coast. Eng. 116, 236–257. https://doi.org/10.1016/j.coastaleng.2016.07.002.

Altomare, C., Suzuki, T., Verwaest, T., 2020. Influence of directional spreading on wave overtopping of sea dikes with gentle and shallow foreshores. Coast. Eng. 157, 103654. https://doi.org/10.1016/j.coastaleng.2020.103654.

Atkinson, A., Baldock, T.E., 2016. A high-resolution sub-aerial and sub-aqueous laser based laboratory beach profile measurement system. Coast. Eng. 107, 28–33. https://doi.org/10.1016/j.coastaleng.2015.10.005.

Booij, N., Ris, R.C., Holthuijsen, L.H., 1999. A third-generation wave model for coastal regions: 1. Model description and validation. J. Geophys. Res.: Oceans 104 (C4), 7649–7666. https://doi.org/10.1029/98JC02622.

Bradbury, A., Allsop, W., Latham, J.-P., Mannion, M., Poole, A., 1988. Rock Armour for Rubble Mound Breawaters, Sea Walls, and Revetments: Recent Progress. H. R. Wallingford.

Brancasi, A., Leone, E., Francone, A., Scaravaglione, G., Tomasicchio, G.R., 2022. On formulae for wave transmission at submerged and low-crested breakwaters. J. Mar. Sci. Eng. 10 (12), 1986. https://doi.org/10.3390/jmse10121986.

Broderick, L.L., Ahrens, J.P., 1982. Riprap Stability Scale Effects. C. E. R. C. (CERC).

Burcharth, H.F., Andersen, T.L., Lara, J.L., 2014. Upgrade of coastal defence structures against increased loadings caused by climate change: a first methodological approach. Coast. Eng. 87, 112–121. https://doi.org/10.1016/j.coastaleng.2013.12.006.

Calabrese, M., Buccino, M., Ciardulli, F., Di Pace, P., Tomasicchio, G.R., Vicinanza, D., 2011. Wave run-up and reflection at rubble mound breakwaters with Ecopodetm armor layer. Coast. Eng. Proceed. 2011. https://doi.org/10.9753/icce.v32.structures.45.

Campos, Á., Castillo, C., Molina-Sanchez, R., 2020a. Damage in rubble mound breakwaters. Part I: historical review of damage models. J. Mar. Sci. Eng. 8 (5), 317. https://doi.org/10.3390/jmse8050317.

Campos, Á., Molina-Sanchez, R., Castillo, C., 2020b. Damage in rubble mound breakwaters. Part II: review of the definition, parameterization, and measurement of damage. J. Mar. Sci. Eng. 8 (5), 306. https://doi.org/10.3390/jmse8050306.

Ciardulli, F., Cuomo, G., Buccino, M., Calabrese, M., 2013. Experimental and numerical investigation on wave transmission past rubble-mound submerged breakwaters. From Sea to Shore–Meeting the Challenges of the Sea. Coasts, Mar. Struct Breakwaters 2013.

CIRIA/CUR/CETMEF, 2007. The rock manual. The Use of Rock in Hydraulic Engineering. CIRIA.

Díaz-Carrasco, P., Molines, J., Gómez-Martín, M.E., Medina, J.R., 2023. Simple and explicit neural network-derived formula to estimate wave reflection on mound breakwaters. Coast. Eng. 186, 104404. https://doi.org/10.1016/j.coastaleng.2023.104404.

Eldrup, M.R., Andersen, T.L., 2019. Extension of shallow water rock armour stability formulae to nonlinear waves. Coast. Eng. 153, 103536. https://doi.org/10.1016/j.coastaleng.2019.103536.

Eldrup, M.R., Lykke Andersen, T., Burcharth, H.F., 2019. Stability of rubble mound breakwaters—a study of the notional permeability factor, based on physical model tests. Water 11 (5), 934. https://doi.org/10.3390/w11050934.

Eldrup, M.R., Andersen, T.L., 2024. Generation of highly nonlinear waves in A short wave flume. CoastLab Proceed. 2024: Phys. Mod. Coast. Eng. Sci. https://doi.org/10.59490/coastlab.2024.687.

Etemad-Shahidi, A., Bali, M., van Gent, M.R.A., 2020. On the stability of rock armored rubble mound structures. Coast. Eng. 158, 103655. https://doi.org/10.1016/j.coastaleng.2020.103655.

Frostick, L.E., McLelland, S.J., Mercer, T.G., 2011. Users guide to physical modelling and experimentation. IAHR Des. Manual.

Goda, Y., 2010a. Random seas and design of maritime structures. World Sci.

Goda, Y., 2010b. Reanalysis of regular and random breaking wave statistics. Coast Eng. J. 52 (1), 71–106. https://doi.org/10.1142/S0578563410002129.

Goda, Y., 2012. Design wave height selection in intermediate-depth waters. Coast Eng. 66, 3–7.

Herrera, M.P., Medina, J.R., 2015. Toe berm design for very shallow water on steep sea bottoms. Coast. Eng. 103, 67–77. https://doi.org/10.1016/j.coastaleng.2015.06.005.

Herrera, M.P., Gomez-Martín, M.E., Medina, J.R., 2017. Hydraulic stability of rock armors in breaking wave conditions. Coast. Eng. 127, 55–67. https://doi.org/10.1016/j.coastaleng.2017.06.010.

Hofland, B., Chen, X., Altomare, C., Oosterlo, P., 2017. Prediction formula for the spectral wave period $T_{m-1,0}$ on mildly sloping shallow foreshores. Coast. Eng. 123, 21–28. https://doi.org/10.1016/j.coastaleng.2017.02.005.

Hudson, R.Y., 1975. Reliability of rubble-mound breakwater stability models. US Army Engineer Waterways Experiment Station.

Hudson, R.Y., 1959. Laboratory investigation of rubble-mound breakwaters. J. Waterw. Harb. Div. 85 (3), 93–121.

Hughes, S.A., 1993. Physical models and laboratory techniques in coastal engineering. World Sci. 7. https://doi.org/10.1142/2154.

Iribarren, R., 1938. Una Fórmula para el Cálculo de los Diques de Escollera.

Kamphuis, J.W., 1996. Experiments on design wave height in shallow water. Coast. Eng. Proceed. 1996. https://doi.org/10.9753/icce.v25.%25p.

Lamberti, A., Tomasicchio, G.R., 1997. Stone mobility and longshore transport at reshaping breakwaters. Coast. Eng. 29 (3–4), 263–289. https://doi.org/10.1016/S0378-3839(96)00027-0.

Latham, J.-P., Mannion, M., Poole, A., Bradbury, A., Allsop, N., 1988. The influence of armourstone shape and rounding on the stability of breakwater armour layers. Coast. Eng. Group Rep. 1. Q. M. College.

Losada, M.Á., 2021. Method to assess the interplay of slope, relative water depth, wave steepness, and sea state persistence in the progression of damage to the rock layer over impermeable dikes. Ocean. Eng. 239, 109904. https://doi.org/10.1016/j.oceaneng.2021.109904.

Losada, M.A., Gimenez-Curto, L.A., 1979. The joint effect of the wave height and period on the stability of rubble mound breakwaters using Iribarren's number. Coast. Eng. 3, 77–96. https://doi.org/10.1016/0378-3839(79)90011-5.

Lykke Andersen, T., Eldrup, M.R., 2024. Applicability of reflection separation algorithms to nonlinear irregular waves over sloping foreshores. In: *CoastLab 2024: Physical Modelling in Coastal Engineering and Science* TU Delft Open. https://doi.org/10.59490/coastlab.2024.685.

Mansard, E.P.D., Funke, E.R., 1980. The measurement of incident and reflected spectra using a least squares method. Coast. Eng. Proceed. 1980. https://doi.org/10.9753/icce.v17.8.

Mares-Nasarre, P., van Gent, M.R.A., Morales-Nápoles, O., 2024. A copula-based model to describe the uncertainty of overtopping variables on mound breakwaters. Coast. Eng. 189, 104483. https://doi.org/10.1016/j.coastaleng.2024.104483.

Marino, S., Scaravaglione, G., Francone, A., Valentini, N., Saponieri, A., Damiani, L., van Gent, M.R.A., Tomasicchio, G., 2022. Laboratory investigation on armour stability for extremely shallow water conditions. Proceedings of the IAHR World Congress. Proceedings of the 39th IAHR World Congress, pp. 5973–5979. https://doi.org/10.3850/iahr-39wc2521711920221364. Code 299039, 2022.

Marino, S., Galantucci, R.A., Saponieri, A., 2023. Measuring rock slope damage on rubble mound breakwater through digital photogrammetry. Measurement 211, 112656. https://doi.org/10.1016/j.measurement.2023.112656.

Melby, J.A., Hughes, S.A., 2003. Armor stability based on wave momentum flux. Coast. Struct. 2003. https://doi.org/10.1061/40733(147)5. *Reston, VA*.

Melby, J.A., Kobayashi, N., 2011. Stone armor damage initiation and progression based on the maximum wave momentum flux. J. Coast Res. 27 (1), 110–119.

Melby, J.A., Massey, T.C., Stehno, A.L., Nadal-Caraballo, N.C., Misra, S., Gonzalez, V.M., Engineer Research and Development Center (US), 2021. Sabine pass to galveston bay, TX pre-construction, engineering and design (PED): coastal storm surge and wave hazard assessment: report 1—background and approach. Coastal and Hydraulics Laboratory. US Army Engineer Research and Development Center, Vicksburg, MS.

Scaravaglione, G., Latham, J.-P., Xiang, J., Francone, A., Tomasicchio, G.R., 2022. Historical overview of the structural integrity of concrete armour units. Coast. Offshore Sci. Eng. 1, 68–98. https://doi.org/10.53256/COSE_220105.

Scaravaglione, G., Marino, S., Francone, A., Damiani, L., Tomasicchio, G.R., Saponieri, A., 2024. Laboratory investigation on pore pressures inside a rubble mound breakwater in depth-limited waters. Appl. Ocean Res. 147, 103988. https://doi.org/10.1016/j.apor.2024.103988.

Shah, A.M., Kamphuis, J.W., 1996. The swash zone: a focus on low frequency motion. Coast. Eng. Proceed. 1996.

Smith, G., Wallast, I., van Gent, M.R.A., 2002. Rock slope stability with shallow foreshores. Coast. Eng. Proceed. 2002. https://doi.org/10.1142/9789812791306_0128.

Thompson, D.M., Shuttler, R.M., 1975. Riprap Design for Wind-Wave Attack, a Laboratory Study in Random Waves. Wallingford report EX707 for CIRIA, H. R. Wallingford.

U. S. A. C. E., 2002. CEM: Coastal Engineering Manual. U.S. Army Corps of Engineers. https://books.google.com/books?id=QLO_jwEACAAJ.

Van der Meer, J.W., 1988. Rock Slopes and Gravel Beaches under Wave Attack. Ph.D. Thesis. Delft Hydraulics.

Van der Meer, J.W., 2021. Rock armour slope stability under wave attack; the Van der Meer Formula revisited. J. Coast. Hydraulic Struct. 1. https://doi.org/10.48438/jchs.2021.0008.

Van Gent, M.R.A., 1999. Physical Model Investigations on Coastal Structures with Shallow Foreshores; 2D Model Tests with Single and Double-Peaked Wave Energy Spectra. Delft Hydraulics Report H3608, December 1999, Delft.

Van Gent, M.R.A., 2001. Wave runup on dikes with shallow foreshores. J. Waterw. Port, Coast. Ocean Eng. 127 (5), 254–262. https://doi.org/10.1061/(ASCE)0733-950X(2001)127:5(254.

Van Gent, M.R.A., 2004. On the stability of rock slopes. Environmentally friendly coastal protection: proceedings of the NATO advanced research workshop on environmentally friendly coastal protection structures Varna, Bulgaria. https://doi.org/10.1007/1-4020-3301-X_5.

Van Gent, M.R.A., Smale, A.J., Kuiper, C., 2003. Stability of rock slopes with shallow foreshores. Coast. Struct. 2003. https://doi.org/10.1061/40733(147)9.

Van Gent, M.R.A., Teng, D.Y.Y., 2023. Climate Adaptation of Coastal Structures: Application of Adaptation Pathways for Rubble Mound Breakwaters. PIANC-COPEDEC 2023, Manila, Philippines.

Vidal, C., Medina, R., Lomónaco, P., 2006. Wave height parameter for damage description of rubble-mound breakwaters. Coast. Eng. 53 (9), 711–722. https://doi.org/10.1016/j.coastaleng.2006.02.007.

Wolters, G., van Gent, M.R.A., Allsop, W., Hamm, L., Mühlestein, D., 2009. HYDRALAB III: guidelines for physical model tests for rubble mound breakwaters. Coast, Mar. Struct. Breakwaters 2009. Edinburgh.
Wolters, G., van Gent, M.R.A., Hofland, B., Wellens, P., 2014. Wave damping and permeability scaling in rubble mound breakwaters. Proc. Coastlab 2014, Varna.
Zelt, J.A., Skjelbreia, J.E., 1992. Estimating incident and reflected wave fields using an arbitrary number of wave gauges. Coast. Eng. Proceed. 1 (23), 777–789. https://doi.org/10.9753/icce.v23.%25p, 1992.

Glossary

α: Structure seaward slope angle **[°]**
γ: Spectrum enhancement factor **[-]**
Δ: Relative buoyant density of the rock armour **[-]**
ξ_m: Surf similarity parameter using H_{m0} and T_m **[-]**
$\xi_{m\text{-}1,0}$: Surf similarity parameter using H_{m0} and $T_{m\text{-}1,0}$ **[-]**
$\xi_{m\text{-}1,0,c}$: Transition surf similarity parameter in EA formula **[-]**
$\xi_{s\text{-}1,0}$: Surf similarity parameter using H_s and $T_{m\text{-}1,0}$ **[-]**
$\xi_{s\text{-}1,0,c}$: Transition surf similarity parameter **[-]**
Π_0: Nonlinearity parameter **[-]**
ρ_r: Density of the armour rock **[Kg/m^3]**
ρ_w: Density of the water **[Kg/m^3]**
A_e: Eroded area **[m^2]**
A_a: Accretion area **[m^2]**
a, b: Regression fitting parameters **[-]**
BLc: Blockiness coefficient **[%]**
c_{VG}, $c_{VG,new}$, c_{EA1}, c_{EA2}, c_{ES1}, c_{ES2}, $c_{ES,new}$: Regression fitting coefficients for the stability equations **[-]**
c_{pl}, c_{su}: Stone shape coefficients **[-]**
C_p: Permeability coefficient, $C_p = \left[1 + \left(\frac{D_{n50,core}}{D_{n50}}\right)^{3/10}\right]^{3/5}$ **[-]**
D_{85}/D_{15}: Grading uniformity coefficient **[-]**
D_{85}: Mass exceeded by 85% of a sample by weight **[m]**
D_{15}: Mass exceeded by 15% of a sample by weight **[m]**
D_{n50}: Armour nominal median stone diameter, $D_{n50} = (M_{50}/\rho_r)^{1/3}$ **[m]**
$D_{n50,core}$: Core nominal median stone diameter **[m]**
$D_{n50,underlayer}$: Underlayer nominal median stone diameter **[m]**
dz: Spatial evolution of slope elevation changes with respect to the initial slope **[m]**
g: Gravity acceleration **[m/s^2]**
h: Water depth at toe of the structure **[m]**
h_r: Relative water depth, h_r=$H_{m0,o}/h$ **[-]**
h_t: Water depth at the end of the transitional slope **[m]**
H_s: Significant wave height in the time domain, H_s=$H_{1/3}$ **[m]**
H_{m0}: Significant (spectral) wave height in frequency domain, H_{m0}=$4(m_0)^{1/2}$ **[m]**
$H_{2\%}$: Wave height exceeded by 2 percent of the waves in time domain **[m]**
$H_{1/50}$: Average wave height of the 50 highest waves in the time domain **[m]**
L_m: Wavelength using T_m **[m]**
$L_{m\text{-}1,0}$: Wavelength using $T_{m\text{-}1,0}$ **[m]**
L_p: Wavelength using T_p **[m]**
LT: Length-to-thickness ratio **[-]**
m: Foreshore slope angle **[°]**
m_0: Zeroth moment of the frequency spectrum **[m^2]**
m_0^{IG}: Infragravity (IG) zeroth moment of the frequency spectrum **[m^2]**
m_0^{TOT}: Total zeroth moment of the frequency spectrum **[m^2]**
M_{50}: Median mass of the armour rock grading **[Kg]**
n: Porosity of the structure core **[-]**
N: Number of observations **[-]**
N_s: Stability number **[-]**
N_w: Number of waves **[-]**
P: Notional permeability factor **[-]**
R_{eA}: Reynolds number at the armour layer **[-]**
R_{ep}: Reynolds number inside the structure core **[-]**
R_c: Crest freeboard above the still water level **[m]**
RMSE: Root Mean Square Error **[-]**
R^2: Determination coefficient **[-]**
S: Damage level **[-]**
s_m: Wave steepness using H_{m0} and T_m **[-]**
$s_{m\text{-}1,0}$: Wave steepness using H_{m0} and $T_{m\text{-}1,0}$ **[-]**
$T_{m\text{-}1,0}$: Negative spectral energy wave period, $T_{m\text{-}1,0}$=m_{-1}/m_0 **[s]**
T_m: Mean period **[s]**
T_p: Peak wave period **[s]**
t_r: Duration of the test **[s]**
x: Longitudinal coordinate positive towards the external side of the structure **[m]**
y: Transversal coordinate positive in the wave propagation direction **[m]**
z: Vertical coordinate positive in the upper direction **[m]**